Observing Application

Date:	Jul 31, 2024
Proposal ID:	VLA/25A-330
Legacy ID:	AA576
PI:	Sean Andrews
Type:	Large
Category:	Star Formation
Total time:	384.3

A Centimeter-band Continuum Survey of Taurus Protoplanetary Disks

Abstract:

We propose a VLA Large Program to measure the complete ~10-45 GHz continuum spectra from a large and diverse sample of Taurus protoplanetary disks. With a modest, complementary Joint request for 100 GHz measurements with ALMA and ancillary archival measurements at higher frequencies, we will robustly disentangle the contributions from thermal dust emission and any radio contamination to measure the dust luminosities and spectral indices in the part of the spectrum that has much lower average optical depths (~30 GHz, or 1 cm wavelength) than is typically probed. The dust spectrum shapes (comparisons of the spectral index in different frequency regimes) and ~1 cm luminosities will be compared in a large sample for the first time, to: assess the impact of optically thick emission on the demographic trends found at ~1 mm (correlations with stellar mass and accretion rate); test and refine the predictions of disk evolution population synthesis models; and make a more accurate assessment of the potential biases from high optical depths in standard estimates of disk masses. We expect these data will have a lasting legacy for ngVLA forecasting and planning, as these nearby, northern-sky disks will be the prime targets for cm-band imaging in the future.

Authors:

Name	Institution	Email	Status
Andrews, Sean	Center for Astrophysics | Harvard & Smithsonian	sandrews@cfa.harvard.edu	
Chandler, Claire	National Radio Astronomy Observatory	cchandle@nrao.edu	
Wilner, David	Center for Astrophysics | Harvard & Smithsonian	dwilner@cfa.harvard.edu	
Macias, Enrique	European Southern Observatory	emacias@eso.org	
Ueda, Takahiro	Center for Astrophysics | Harvard & Smithsonian	takahiro.ueda@cfa.harvard.edu	
Long, Feng	Arizona, University of	fenglong@email.arizona.edu	
Birnstiel, Tilman	MÃ¼nchen, Ludwig-Maximilians-UniversitÃ¤t	til.birnstiel@lmu.de	
Carrasco-Gonzalez, Carlos	MÃ©xico, Universidad Nacional AutÃ³noma de	c.carrasco@irya.unam.mx	
Liu, Hauyu	National Sun Yat-sen University	baobabyoo@gmail.com	

Principal Investigator: Sean Andrews
Contact: Sean Andrews
Telephone: 617-496-7645
Email: sandrews@cfa.harvard.edu

Related Proposals:

Joint:

Joint with ALMA. ALMA Hours: 7.

Observing type(s):

Continuum

VLA Resources

Name	Conf.	Frontend & Backend	Setup
Q-phot	D	Q Band 0.7 cm 40000 - 50000 MHz General and Shared Risk Observing - Wideband	Basebands: 4 x 2 GHz(3-bit) Baseband centers (GHz): 41, 43, 45, 47 Total bandwidth (GHz): 8.0 Polarization products: Full Dump time (s): 3.0 Data rate: 15.8 MB/s, 56.9 GB/h
Ka-phot	D	Ka Band 0.9 cm 26500 - 40000 MHz General and Shared Risk Observing - Wideband	Basebands: 4 x 2 GHz(3-bit) Baseband centers (GHz): 30, 32, 34, 36 Total bandwidth (GHz): 8.0 Polarization products: Full Dump time (s): 3.0 Data rate: 15.8 MB/s, 56.9 GB/h
K-phot	C	K Band 1.3 cm 18000 - 26500 MHz General and Shared Risk Observing - Wideband	Basebands: 4 x 2 GHz(3-bit) Baseband centers (GHz): 19, 21, 23, 25 Total bandwidth (GHz): 8.0 Polarization products: Full Dump time (s): 3.0 Data rate: 15.8 MB/s, 56.9 GB/h
X-phot	C	X Band 3.6 cm 8000 - 12000 MHz General and Shared Risk Observing - Wideband	Basebands: 2 x 2 GHz(3-bit) Baseband centers (GHz): 9, 11 Total bandwidth (GHz): 4.0 Polarization products: Full Dump time (s): 3.0 Data rate: 7.9 MB/s, 28.4 GB/h
Ku-phot	C	Ku Band 2 cm 12000 - 18000 MHz General and Shared Risk Observing - Wideband	Basebands: 3 x 2 GHz(3-bit) Baseband centers (GHz): 13, 15, 17 Total bandwidth (GHz): 6.0 Polarization products: Full Dump time (s): 3.0 Data rate: 11.8 MB/s, 42.6 GB/h

Sources

Name	Position		Velocity		Group
FM_Tau	Coordinate system	Equatorial	Convention	Radio	Group1
	Equinox	J2000			
	Right Ascension	04:14:13.584	Ref. frame	LSRK	
		00:00:00			
	Declination	+28:12:49.170	Velocity	0	
		00:00:00			
	Calibrator	No			
FN_Tau	Coordinate system	Equatorial	Convention	Radio	Group1
	Equinox	J2000			
	Right Ascension	04:14:14.595	Ref. frame	LSRK	
		00:00:00			
	Declination	+28:27:58.068	Velocity	0	
		00:00:00			
	Calibrator	No			
CW_Tau	Coordinate system	Equatorial	Convention	Radio	Group1
	Equinox	J2000			
	Right Ascension	04:14:17.004	Ref. frame	LSRK	
		00:00:00			
	Declination	+28:10:57.767	Velocity	0	
		00:00:00			
	Calibrator	No			
CIDA_1	Coordinate system	Equatorial	Convention	Radio	Group1
	Equinox	J2000			
	Right Ascension	04:14:17.610	Ref. frame	LSRK	
		00:00:00			
	Declination	+28:06:09.655	Velocity	0	
		00:00:00			
	Calibrator	No			
MHO_1	Coordinate system	Equatorial	Convention	Radio	Group1
	Equinox	J2000			
	Right Ascension	04:14:26.268	Ref. frame	LSRK	
		00:00:00			
	Declination	+28:06:03.271	Velocity	0	
		00:00:00			
	Calibrator	No			
MHO_2	Coordinate system	Equatorial	Convention	Radio	Group1
	Equinox	J2000			
	Right Ascension	04:14:26.401	Ref. frame	LSRK	
		00:00:00			
	Declination	+28:05:59.636	Velocity	0	
		00:00:00			
	Calibrator	No			

Name	Position		Velocity		Group
MHO_3	Coordinate system	Equatorial	Convention	Radio	Group1
	Equinox	J2000			
	Right Ascension	04:14:30.551	Ref. frame	LSRK	
		00:00:00			
	Declination	+28:05:14.597	Velocity	0	
		00:00:00			
	Calibrator	No			
FP_Tau	Coordinate system	Equatorial	Convention	Radio	Group1
	Equinox	J2000			
	Right Ascension	04:14:47.303	Ref. frame	LSRK	
		00:00:00			
	Declination	+26:46:26.414	Velocity	0	
		00:00:00			
	Calibrator	No			
CX_Tau	Coordinate system	Equatorial	Convention	Radio	Group1
	Equinox	J2000			
	Right Ascension	04:14:47.862	Ref. frame	LSRK	
		00:00:00			
	Declination	+26:48:11.015	Velocity	0	
		00:00:00			
	Calibrator	No			
J04153916	Coordinate system	Equatorial	Convention	Radio	Group1
	Equinox	J2000			
	Right Ascension	04:15:39.163	Ref. frame	LSRK	
		00:00:00			
	Declination	+28:18:58.525	Velocity	0	
		00:00:00			
	Calibrator	No			
IRAS_04125+2902	Coordinate system	Equatorial	Convention	Radio	Group1
	Equinox	J2000			
	Right Ascension	04:15:42.787	Ref. frame	LSRK	
		00:00:00			
	Declination	+29:09:59.832	Velocity	0	
		00:00:00			
	Calibrator	No			
J04155799	Coordinate system	Equatorial	Convention	Radio	Group1
	Equinox	J2000			
	Right Ascension	04:15:57.999	Ref. frame	LSRK	
		00:00:00			
	Declination	+27:46:17.332	Velocity	0	
		00:00:00			
	Calibrator	No			

Name	Position		Velocity		Group
J04161210	Coordinate system	Equatorial	Convention	Radio	Group1
	Equinox	J2000			
	Right Ascension	04:16:12.108	Ref. frame	LSRK	
		00:00:00			
	Declination	+27:56:38.480	Velocity	0	
		00:00:00			
	Calibrator	No			
CY_Tau	Coordinate system	Equatorial	Convention	Radio	Group1
	Equinox	J2000			
	Right Ascension	04:17:33.728	Ref. frame	LSRK	
		00:00:00			
	Declination	+28:20:46.812	Velocity	0	
		00:00:00			
	Calibrator	No			
KPNO_10	Coordinate system	Equatorial	Convention	Radio	Group1
	Equinox	J2000			
	Right Ascension	04:17:49.557	Ref. frame	LSRK	
		00:00:00			
	Declination	+28:13:31.770	Velocity	0	
		00:00:00			
	Calibrator	No			
V409_Tau	Coordinate system	Equatorial	Convention	Radio	Group1
	Equinox	J2000			
	Right Ascension	04:18:10.783	Ref. frame	LSRK	
		00:00:00			
	Declination	+25:19:57.381	Velocity	0	
		00:00:00			
	Calibrator	No			
V410_X-ray_2	Coordinate system	Equatorial	Convention	Radio	Group1
	Equinox	J2000			
	Right Ascension	04:18:34.447	Ref. frame	LSRK	
		00:00:00			
	Declination	+28:30:30.226	Velocity	0	
		00:00:00			
	Calibrator	No			
V892_Tau	Coordinate system	Equatorial	Convention	Radio	Group1
	Equinox	J2000			
	Right Ascension	04:18:40.616	Ref. frame	LSRK	
		00:00:00			
	Declination	+28:19:15.625	Velocity	0	
		00:00:00			
	Calibrator	No			

Name	Position		Velocity		Group
LR_1	Coordinate system	Equatorial	Convention	Radio	Group1
	Equinox	J2000			
	Right Ascension	04:18:41.332	Ref. frame	LSRK	
		00:00:00			
	Declination	+28:27:25.009	Velocity	0	
		00:00:00			
	Calibrator	No			
V410_X-ray_7	Coordinate system	Equatorial	Convention	Radio	Group1
	Equinox	J2000			
	Right Ascension	04:18:42.501	Ref. frame	LSRK	
		00:00:00			
	Declination	+28:18:49.923	Velocity	0	
		00:00:00			
	Calibrator	No			
BP_Tau	Coordinate system	Equatorial	Convention	Radio	Group1
	Equinox	J2000			
	Right Ascension	04:19:15.834	Ref. frame	LSRK	
		00:00:00			
	Declination	+29:06:26.927	Velocity	0	
		00:00:00			
	Calibrator	No			
J04202144	Coordinate system	Equatorial	Convention	Radio	Group1
	Equinox	J2000			
	Right Ascension	04:20:21.443	Ref. frame	LSRK	
		00:00:00			
	Declination	+28:13:49.174	Velocity	0	
		00:00:00			
	Calibrator	No			
J04202555	Coordinate system	Equatorial	Convention	Radio	Group1
	Equinox	J2000			
	Right Ascension	04:20:25.557	Ref. frame	LSRK	
		00:00:00			
	Declination	+27:00:35.548	Velocity	0	
		00:00:00			
	Calibrator	No			
IRAS_04187+1927	Coordinate system	Equatorial	Convention	Radio	Group1
	Equinox	J2000			
	Right Ascension	04:21:43.235	Ref. frame	LSRK	
		00:00:00			
	Declination	+19:34:13.311	Velocity	0	
		00:00:00			
	Calibrator	No			

Name	Position		Velocity		Group
DE_Tau	Coordinate system	Equatorial	Convention	Radio	Group1
	Equinox	J2000			
	Right Ascension	04:21:55.635	Ref. frame	LSRK	
		00:00:00			
	Declination	+27:55:06.184	Velocity	0	
		00:00:00			
	Calibrator	No			
IRAS_04196+2638	Coordinate system	Equatorial	Convention	Radio	Group1
	Equinox	J2000			
	Right Ascension	04:22:47.880	Ref. frame	LSRK	
		00:00:00			
	Declination	+26:45:52.873	Velocity	0	
		00:00:00			
	Calibrator	No			
IRAS_04200+2759	Coordinate system	Equatorial	Convention	Radio	Group1
	Equinox	J2000			
	Right Ascension	04:23:07.776	Ref. frame	LSRK	
		00:00:00			
	Declination	+28:05:57.467	Velocity	0	
		00:00:00			
	Calibrator	No			
IP_Tau	Coordinate system	Equatorial	Convention	Radio	Group1
	Equinox	J2000			
	Right Ascension	04:24:57.082	Ref. frame	LSRK	
		00:00:00			
	Declination	+27:11:56.540	Velocity	0	
		00:00:00			
	Calibrator	No			
DF_Tau	Coordinate system	Equatorial	Convention	Radio	Group1
	Equinox	J2000			
	Right Ascension	04:27:02.793	Ref. frame	LSRK	
		00:00:00			
	Declination	+25:42:22.453	Velocity	0	
		00:00:00			
	Calibrator	No			
DG_Tau	Coordinate system	Equatorial	Convention	Radio	Group1
	Equinox	J2000			
	Right Ascension	04:27:04.692	Ref. frame	LSRK	
		00:00:00			
	Declination	+26:06:16.060	Velocity	0	
		00:00:00			
	Calibrator	No			

Name	Position		Velocity		Group
IRAS_04260+2642	Coordinate system	Equatorial	Convention	Radio	Group2
	Equinox	J2000			
	Right Ascension	04:29:04.983	Ref. frame	LSRK	
		00:00:00			
	Declination	+26:49:07.188	Velocity	0	
		00:00:00			
	Calibrator	No			
IRAS_04263+2654	Coordinate system	Equatorial	Convention	Radio	Group2
	Equinox	J2000			
	Right Ascension	04:29:21.662	Ref. frame	LSRK	
		00:00:00			
	Declination	+27:01:25.516	Velocity	0	
		00:00:00			
	Calibrator	No			
XEST_13-010	Coordinate system	Equatorial	Convention	Radio	Group2
	Equinox	J2000			
	Right Ascension	04:29:36.065	Ref. frame	LSRK	
		00:00:00			
	Declination	+24:35:55.589	Velocity	0	
		00:00:00			
	Calibrator	No			
IQ_Tau	Coordinate system	Equatorial	Convention	Radio	Group2
	Equinox	J2000			
	Right Ascension	04:29:51.557	Ref. frame	LSRK	
		00:00:00			
	Declination	+26:06:44.860	Velocity	0	
		00:00:00			
	Calibrator	No			
J04295950	Coordinate system	Equatorial	Convention	Radio	Group2
	Equinox	J2000			
	Right Ascension	04:29:59.508	Ref. frame	LSRK	
		00:00:00			
	Declination	+24:33:07.686	Velocity	0	
		00:00:00			
	Calibrator	No			
UX_Tau_A	Coordinate system	Equatorial	Convention	Radio	Group2
	Equinox	J2000			
	Right Ascension	04:30:03.996	Ref. frame	LSRK	
		00:00:00			
	Declination	+18:13:49.436	Velocity	0	
		00:00:00			
	Calibrator	No			

Name	Position		Velocity		Group
ZZ_Tau_IRS	Coordinate system	Equatorial	Convention	Radio	Group2
	Equinox	J2000			
	Right Ascension	04:30:51.721	Ref. frame	LSRK	
		00:00:00			
	Declination	+24:41:47.457	Velocity	0	
		00:00:00			
	Calibrator	No			
Haro_6-13	Coordinate system	Equatorial	Convention	Radio	Group2
	Equinox	J2000			
	Right Ascension	04:32:15.417	Ref. frame	LSRK	
		00:00:00			
	Declination	+24:28:59.578	Velocity	0	
		00:00:00			
	Calibrator	No			
MHO_6	Coordinate system	Equatorial	Convention	Radio	Group2
	Equinox	J2000			
	Right Ascension	04:32:22.110	Ref. frame	LSRK	
		00:00:00			
	Declination	+18:27:42.650	Velocity	0	
		00:00:00			
	Calibrator	No			
GG_Tau_A	Coordinate system	Equatorial	Convention	Radio	Group2
	Equinox	J2000			
	Right Ascension	04:32:30.351	Ref. frame	LSRK	
		00:00:00			
	Declination	+17:31:40.494	Velocity	0	
		00:00:00			
	Calibrator	No			
FY_Tau	Coordinate system	Equatorial	Convention	Radio	Group2
	Equinox	J2000			
	Right Ascension	04:32:30.578	Ref. frame	LSRK	
		00:00:00			
	Declination	+24:19:57.360	Velocity	0	
		00:00:00			
	Calibrator	No			
FZ_Tau	Coordinate system	Equatorial	Convention	Radio	Group2
	Equinox	J2000			
	Right Ascension	04:32:31.763	Ref. frame	LSRK	
		00:00:00			
	Declination	+24:20:03.056	Velocity	0	
		00:00:00			
	Calibrator	No			

Name	Position		Velocity		Group
UZ_Tau_E	Coordinate system	Equatorial	Convention	Radio	Group2
	Equinox	J2000			
	Right Ascension	04:32:43.072	Ref. frame	LSRK	
		00:00:00			
	Declination	+25:52:31.014	Velocity	0	
		00:00:00			
	Calibrator	No			
V807_Tau	Coordinate system	Equatorial	Convention	Radio	Group2
	Equinox	J2000			
	Right Ascension	04:33:06.636	Ref. frame	LSRK	
		00:00:00			
	Declination	+24:09:54.978	Velocity	0	
		00:00:00			
	Calibrator	No			
IRAS_04301+2608	Coordinate system	Equatorial	Convention	Radio	Group2
	Equinox	J2000			
	Right Ascension	04:33:14.362	Ref. frame	LSRK	
		00:00:00			
	Declination	+26:14:23.464	Velocity	0	
		00:00:00			
	Calibrator	No			
J04333278	Coordinate system	Equatorial	Convention	Radio	Group2
	Equinox	J2000			
	Right Ascension	04:33:32.807	Ref. frame	LSRK	
		00:00:00			
	Declination	+18:00:43.605	Velocity	0	
		00:00:00			
	Calibrator	No			
GI_Tau	Coordinate system	Equatorial	Convention	Radio	Group2
	Equinox	J2000			
	Right Ascension	04:33:34.061	Ref. frame	LSRK	
		00:00:00			
	Declination	+24:21:17.069	Velocity	0	
		00:00:00			
	Calibrator	No			
GK_Tau	Coordinate system	Equatorial	Convention	Radio	Group2
	Equinox	J2000			
	Right Ascension	04:33:34.563	Ref. frame	LSRK	
		00:00:00			
	Declination	+24:21:05.855	Velocity	0	
		00:00:00			
	Calibrator	No			

Name	Position		Velocity		Group
J04333905	Coordinate system	Equatorial	Convention	Radio	Group2
	Equinox	J2000			
	Right Ascension	04:33:39.077	Ref. frame	LSRK	
		00:00:00			
	Declination	+22:27:20.443	Velocity	0	
		00:00:00			
	Calibrator	No			
J04334171	Coordinate system	Equatorial	Convention	Radio	Group2
	Equinox	J2000			
	Right Ascension	04:33:41.727	Ref. frame	LSRK	
		00:00:00			
	Declination	+17:50:40.139	Velocity	0	
		00:00:00			
	Calibrator	No			
J04334465	Coordinate system	Equatorial	Convention	Radio	Group2
	Equinox	J2000			
	Right Ascension	04:33:44.659	Ref. frame	LSRK	
		00:00:00			
	Declination	+26:15:00.436	Velocity	0	
		00:00:00			
	Calibrator	No			
DM_Tau	Coordinate system	Equatorial	Convention	Radio	Group2
	Equinox	J2000			
	Right Ascension	04:33:48.734	Ref. frame	LSRK	
		00:00:00			
	Declination	+18:10:09.973	Velocity	0	
		00:00:00			
	Calibrator	No			
AA_Tau	Coordinate system	Equatorial	Convention	Radio	Group2
	Equinox	J2000			
	Right Ascension	04:34:55.420	Ref. frame	LSRK	
		00:00:00			
	Declination	+24:28:53.034	Velocity	0	
		00:00:00			
	Calibrator	No			
HO_Tau	Coordinate system	Equatorial	Convention	Radio	Group2
	Equinox	J2000			
	Right Ascension	04:35:20.210	Ref. frame	LSRK	
		00:00:00			
	Declination	+22:32:14.561	Velocity	0	
		00:00:00			
	Calibrator	No			

Name	Position		Velocity		Group
DN_Tau	Coordinate system	Equatorial	Convention	Radio	Group2
	Equinox	J2000			
	Right Ascension	04:35:27.378	Ref. frame	LSRK	
		00:00:00			
	Declination	+24:14:58.910	Velocity	0	
		00:00:00			
	Calibrator	No			
HP_Tau	Coordinate system	Equatorial	Convention	Radio	Group2
	Equinox	J2000			
	Right Ascension	04:35:52.782	Ref. frame	LSRK	
		00:00:00			
	Declination	+22:54:23.157	Velocity	0	
		00:00:00			
	Calibrator	No			
DO_Tau	Coordinate system	Equatorial	Convention	Radio	Group2
	Equinox	J2000			
	Right Ascension	04:38:28.588	Ref. frame	LSRK	
		00:00:00			
	Declination	+26:10:49.468	Velocity	0	
		00:00:00			
	Calibrator	No			
HV_Tau_C	Coordinate system	Equatorial	Convention	Radio	Group2
	Equinox	J2000			
	Right Ascension	04:38:35.290	Ref. frame	LSRK	
		00:00:00			
	Declination	+26:10:38.640	Velocity	0	
		00:00:00			
	Calibrator	No			
J04385859	Coordinate system	Equatorial	Convention	Radio	Group2
	Equinox	J2000			
	Right Ascension	04:38:58.602	Ref. frame	LSRK	
		00:00:00			
	Declination	+23:36:35.152	Velocity	0	
		00:00:00			
	Calibrator	No			
J04393364	Coordinate system	Equatorial	Convention	Radio	Group2
	Equinox	J2000			
	Right Ascension	04:39:33.641	Ref. frame	LSRK	
		00:00:00			
	Declination	+23:59:21.221	Velocity	0	
		00:00:00			
	Calibrator	No			

Name	Position		Velocity		Group
ITG_15	Coordinate system	Equatorial	Convention	Radio	Group2
	Equinox	J2000			
	Right Ascension	04:39:44.881	Ref. frame	LSRK	
		00:00:00			
	Declination	+26:01:52.706	Velocity	0	
		00:00:00			
	Calibrator	No			
IRAS_04370+2559	Coordinate system	Equatorial	Convention	Radio	Group2
	Equinox	J2000			
	Right Ascension	04:40:08.005	Ref. frame	LSRK	
		00:00:00			
	Declination	+26:05:25.434	Velocity	0	
		00:00:00			
	Calibrator	No			
ITG_33A	Coordinate system	Equatorial	Convention	Radio	Group2
	Equinox	J2000			
	Right Ascension	04:41:08.264	Ref. frame	LSRK	
		00:00:00			
	Declination	+25:56:07.358	Velocity	0	
		00:00:00			
	Calibrator	No			
CoKu_Tau_4	Coordinate system	Equatorial	Convention	Radio	Group2
	Equinox	J2000			
	Right Ascension	04:41:16.810	Ref. frame	LSRK	
		00:00:00			
	Declination	+28:40:00.074	Velocity	0	
		00:00:00			
	Calibrator	No			
IRAS_04385+2550	Coordinate system	Equatorial	Convention	Radio	Group2
	Equinox	J2000			
	Right Ascension	04:41:38.826	Ref. frame	LSRK	
		00:00:00			
	Declination	+25:56:26.741	Velocity	0	
		00:00:00			
	Calibrator	No			
CIDA_7	Coordinate system	Equatorial	Convention	Radio	Group2
	Equinox	J2000			
	Right Ascension	04:42:21.022	Ref. frame	LSRK	
		00:00:00			
	Declination	+25:20:34.306	Velocity	0	
		00:00:00			
	Calibrator	No			

Name	Position		Velocity		Group
GO_Tau	Coordinate system	Equatorial	Convention	Radio	Group2
	Equinox	J2000			
	Right Ascension	04:43:03.076	Ref. frame	LSRK	
		00:00:00			
	Declination	+25:20:18.707	Velocity	0	
		00:00:00			
	Calibrator	No			
IRAS_04414+2506	Coordinate system	Equatorial	Convention	Radio	Group2
	Equinox	J2000			
	Right Ascension	04:44:27.143	Ref. frame	LSRK	
		00:00:00			
	Declination	+25:12:16.435	Velocity	0	
		00:00:00			
	Calibrator	No			
IRAS_04429+1550	Coordinate system	Equatorial	Convention	Radio	Group2
	Equinox	J2000			
	Right Ascension	04:45:51.351	Ref. frame	LSRK	
		00:00:00			
	Declination	+15:55:36.662	Velocity	0	
		00:00:00			
	Calibrator	No			
DQ_Tau	Coordinate system	Equatorial	Convention	Radio	Group2
	Equinox	J2000			
	Right Ascension	04:46:53.058	Ref. frame	LSRK	
		00:00:00			
	Declination	+17:00:00.136	Velocity	0	
		00:00:00			
	Calibrator	No			
Haro_6-37_C	Coordinate system	Equatorial	Convention	Radio	Group2
	Equinox	J2000			
	Right Ascension	04:46:58.980	Ref. frame	LSRK	
		00:00:00			
	Declination	+17:02:38.195	Velocity	0	
		00:00:00			
	Calibrator	No			
DS_Tau	Coordinate system	Equatorial	Convention	Radio	Group2
	Equinox	J2000			
	Right Ascension	04:47:48.595	Ref. frame	LSRK	
		00:00:00			
	Declination	+29:25:11.192	Velocity	0	
		00:00:00			
	Calibrator	No			

Name	Position		Velocity		Group
SU_Aur	Coordinate system	Equatorial	Convention	Radio	Group3
	Equinox	J2000			
	Right Ascension	04:55:59.387	Ref. frame	LSRK	
		00:00:00			
	Declination	+30:34:01.500	Velocity	0	
		00:00:00			
	Calibrator	No			
V836_Tau	Coordinate system	Equatorial	Convention	Radio	Group3
	Equinox	J2000			
	Right Ascension	05:03:06.599	Ref. frame	LSRK	
		00:00:00			
	Declination	+25:23:19.607	Velocity	0	
		00:00:00			
	Calibrator	No			
CIDA_8	Coordinate system	Equatorial	Convention	Radio	Group3
	Equinox	J2000			
	Right Ascension	05:04:41.397	Ref. frame	LSRK	
		00:00:00			
	Declination	+25:09:54.583	Velocity	0	
		00:00:00			
	Calibrator	No			
MWC_758	Coordinate system	Equatorial	Convention	Radio	Group3
	Equinox	J2000			
	Right Ascension	05:30:27.529	Ref. frame	LSRK	
		00:00:00			
	Declination	+25:19:57.076	Velocity	0	
		00:00:00			
	Calibrator	No			
CQ_Tau	Coordinate system	Equatorial	Convention	Radio	Group3
	Equinox	J2000			
	Right Ascension	05:35:58.467	Ref. frame	LSRK	
		00:00:00			
	Declination	+24:44:54.091	Velocity	0	
		00:00:00			
	Calibrator	No			
AB_Aur	Coordinate system	Equatorial	Convention	Radio	Group3
	Equinox	J2000			
	Right Ascension	04:55:45.846	Ref. frame	LSRK	
		00:00:00.0			
	Declination	+30:33:04.292	Velocity	0.00	
		00:00:00.0			
	Calibrator	No			

Sessions:

Name	Session time (hours)	Repeat	Separation	LST minimum	LST maximum	Elevation minimum
Q group 1	10.7	2	0 day	23:28:49	09:07:45	30
Ka group 1	14.2	2	0 day	23:28:49	09:07:45	30
K group 1	21.4	2	0 day	23:28:49	09:07:45	30
Ku group 1	16.8	2	0 day	22:37:33	09:58:37	20
X group 1	23.2	2	0 day	22:37:33	09:58:37	20
Q group 2	12.5	2	0 day	23:47:03	09:35:14	30
Ka group 2	16.5	2	0 day	23:47:03	09:35:14	30
K group 2	25.2	2	0 day	23:47:03	09:35:14	30
Ku group 2	20.2	2	0 day	22:56:33	10:26:36	20
X group 2	27.9	2	0 day	22:56:33	10:26:36	20
Q group 3	1.0	1	0 day	00:05:58	10:13:21	30
Ka group 3	1.2	1	0 day	00:05:58	10:13:21	30
K group 3	1.5	1	0 day	00:05:58	10:13:21	30
Ku group 3	1.6	1	0 day	23:14:07	11:03:09	20
X group 3	1.8	1	0 day	23:14:07	11:03:09	20

Session Constraints:

Name	Scheduling constraints	Comments
Q group 1		
Ka group 1		
K group 1		
Ku group 1		
X group 1		
Q group 2		
Ka group 2		
K group 2		
Ku group 2		
X group 2		
Q group 3		fractional overhead higher as appropriate for shorter scheduling blocks
Ka group 3		fractional overhead higher as appropriate for shorter scheduling blocks
K group 3		fractional overhead higher as appropriate for shorter scheduling blocks
Ku group 3		fractional overhead higher as appropriate for shorter scheduling blocks
X group 3		

Session Source/Resource Pairs:

Session name	Source	Resource	Time
Q group 1	FM_Tau FN_Tau CW_Tau CIDA_1 MHO_1 MHO_2 MHO_3 FP_Tau CX_Tau J04153916 IRAS_04125+2902 J04155799 J04161210 CY_Tau KPNO_10 V409_Tau V410_X-ray_2 V892_Tau LR_1 V410_X-ray_7 BP_Tau J04202144 J04202555 IRAS_04187+1927 DE_Tau IRAS_04196+2638 IRAS_04200+2759 IP_Tau DF_Tau DG_Tau	Q-phot	10.7 hour
Ka group 1	FM_Tau FN_Tau CW_Tau CIDA_1 MHO_1 MHO_2 MHO_3 FP_Tau CX_Tau J04153916 IRAS_04125+2902 J04155799 J04161210 CY_Tau KPNO_10 V409_Tau V410_X-ray_2 V892_Tau LR_1 V410_X-ray_7 BP_Tau J04202144	Ka-phot	14.2 hour

Session name	Source	Resource	Time
	J04202555 IRAS_04187+1927 DE_Tau IRAS_04196+2638 IRAS_04200+2759 IP_Tau DF_Tau DG_Tau		
K group 1	FM_Tau FN_Tau CW_Tau CIDA_1 MHO_1 MHO_2 MHO_3 FP_Tau CX_Tau J04153916 IRAS_04125+2902 J04155799 J04161210 CY_Tau KPNO_10 V409_Tau V410_X-ray_2 V892_Tau LR_1 V410_X-ray_7 BP_Tau J04202144 J04202555 IRAS_04187+1927 DE_Tau IRAS_04196+2638 IRAS_04200+2759 IP_Tau DF_Tau DG_Tau	K-phot	21.4 hour
Ku group 1	FM_Tau FN_Tau CW_Tau CIDA_1 MHO_1 MHO_2 MHO_3 FP_Tau CX_Tau J04153916 IRAS_04125+2902 J04155799 J04161210 CY_Tau KPNO_10 V409_Tau	Ku-phot	16.8 hour

Session name	Source	Resource	Time
	V410_X-ray_2 V892_Tau LR_1 V410_X-ray_7 BP_Tau J04202144 J04202555 IRAS_04187+1927 DE_Tau IRAS_04196+2638 IRAS_04200+2759 IP_Tau DF_Tau DG_Tau		
X group 1	FM_Tau FN_Tau CW_Tau CIDA_1 MHO_1 MHO_2 MHO_3 FP_Tau CX_Tau J04153916 IRAS_04125+2902 J04155799 J04161210 CY_Tau KPNO_10 V409_Tau V410_X-ray_2 V892_Tau LR_1 V410_X-ray_7 BP_Tau J04202144 J04202555 IRAS_04187+1927 DE_Tau IRAS_04196+2638 IRAS_04200+2759 IP_Tau DF_Tau DG_Tau	X-phot	23.2 hour
Q group 2	IRAS_04260+2642 IRAS_04263+2654 XEST_13-010 IQ_Tau J04295950 UX_Tau_A ZZ_Tau_IRS Haro_6-13 MHO_6 GG_Tau_A	Q-phot	12.5 hour

Session name	Source	Resource	Time
	FY_Tau FZ_Tau UZ_Tau_E V807_Tau IRAS_04301+2608 J04333278 GI_Tau GK_Tau J04333905 J04334171 J04334465 DM_Tau AA_Tau HO_Tau DN_Tau HP_Tau DO_Tau HV_Tau_C J04385859 J04393364 ITG_15 IRAS_04370+2559 ITG_33A CoKu_Tau_4 IRAS_04385+2550 CIDA_7 GO_Tau IRAS_04414+2506 IRAS_04429+1550 DQ_Tau Haro_6-37_C DS_Tau		
Ka group 2	IRAS_04260+2642 IRAS_04263+2654 XEST_13-010 IQ_Tau J04295950 UX_Tau_A ZZ_Tau_IRS Haro_6-13 MHO_6 GG_Tau_A FY_Tau FZ_Tau UZ_Tau_E V807_Tau IRAS_04301+2608 J04333278 GI_Tau GK_Tau J04333905 J04334171 J04334465 DM_Tau	Ka-phot	16.5 hour

Session name	Source	Resource	Time
	AA_Tau HO_Tau DN_Tau HP_Tau DO_Tau HV_Tau_C J04385859 J04393364 ITG_15 IRAS_04370+2559 ITG_33A CoKu_Tau_4 IRAS_04385+2550 CIDA_7 GO_Tau IRAS_04414+2506 IRAS_04429+1550 DQ_Tau Haro_6-37_C DS_Tau		
K group 2	IRAS_04260+2642 IRAS_04263+2654 XEST_13-010 IQ_Tau J04295950 UX_Tau_A ZZ_Tau_IRS Haro_6-13 MHO_6 GG_Tau_A FY_Tau FZ_Tau UZ_Tau_E V807_Tau IRAS_04301+2608 J04333278 GI_Tau GK_Tau J04333905 J04334171 J04334465 DM_Tau AA_Tau HO_Tau DN_Tau HP_Tau DO_Tau HV_Tau_C J04385859 J04393364 ITG_15 IRAS_04370+2559 ITG_33A CoKu_Tau_4	K-phot	25.2 hour

Session name	Source	Resource	Time
	IRAS_04385+2550 CIDA_7 GO_Tau IRAS_04414+2506 IRAS_04429+1550 DQ_Tau Haro_6-37_C DS_Tau		
Ku group 2	IRAS_04260+2642 IRAS_04263+2654 XEST_13-010 IQ_Tau J04295950 UX_Tau_A ZZ_Tau_IRS Haro_6-13 MHO_6 GG_Tau_A FY_Tau FZ_Tau UZ_Tau_E V807_Tau IRAS_04301+2608 J04333278 GI_Tau GK_Tau J04333905 J04334171 J04334465 DM_Tau AA_Tau HO_Tau DN_Tau HP_Tau DO_Tau HV_Tau_C J04385859 J04393364 ITG_15 IRAS_04370+2559 ITG_33A CoKu_Tau_4 IRAS_04385+2550 CIDA_7 GO_Tau IRAS_04414+2506 IRAS_04429+1550 DQ_Tau Haro_6-37_C DS_Tau	Ku-phot	20.2 hour
X group 2	IRAS_04260+2642 IRAS_04263+2654 XEST_13-010 IQ_Tau	X-phot	27.9 hour

Session name	Source	Resource	Time
	J04295950 UX_Tau_A ZZ_Tau_IRS Haro_6-13 MHO_6 GG_Tau_A FY_Tau FZ_Tau UZ_Tau_E V807_Tau IRAS_04301+2608 J04333278 GI_Tau GK_Tau J04333905 J04334171 J04334465 DM_Tau AA_Tau HO_Tau DN_Tau HP_Tau DO_Tau HV_Tau_C J04385859 J04393364 ITG_15 IRAS_04370+2559 ITG_33A CoKu_Tau_4 IRAS_04385+2550 CIDA_7 GO_Tau IRAS_04414+2506 IRAS_04429+1550 DQ_Tau Haro_6-37_C DS_Tau		
Q group 3	SU_Aur V836_Tau CIDA_8 MWC_758 CQ_Tau AB_Aur	Q-phot	1.0 hour
Ka group 3	SU_Aur V836_Tau CIDA_8 MWC_758 CQ_Tau AB_Aur	Ka-phot	1.2 hour
K group 3	SU_Aur V836_Tau CIDA_8 MWC_758	K-phot	1.5 hour

Session name	Source	Resource	Time
	CQ_Tau AB_Aur		
Ku group 3	SU_Aur V836_Tau CIDA_8 MWC_758 CQ_Tau AB_Aur	Ku-phot	1.6 hour
X group 3	SU_Aur V836_Tau CIDA_8 MWC_758 CQ_Tau AB_Aur	X-phot	1.8 hour

Plan of dissertation: no

Technical Justification:

Combined telescopes:

No

Array configuration:

These are photometric measurements of the unresolved spectra of disks. The D configuration provides sufficiently coarse resolution at the high frequencies (Q, Ka) that the target emission will be unresolved (maximum sizes are ~1"), so sensitivity is optimized. The lower frequencies (Ku, X) should be observed in the C configuration, to mitigate any potential confusion from background sources. The K-band data could be conducted in either the D or C configuration, to facilitate flexibility in scheduling.

Subarrays:

N/A

Future semesters:

It would be acceptable to carry over the observations into the next configuration cycle (2026A for D and 2026B for C) if necessary to facilitate scheduling. We will make sure to observe the same sources in all bands in a single configuration cycle in this event, to minimize the potential for bias from variability.

Scheduling restrictions:

The targets (at RA ~ 4-5.5 hours) are accessible in 2025A early in the night in D configuration and late in the night for C configuration. If conditions are unsuitable to complete the survey in 2025A, it is acceptable to finish the observations in the next configuration cycle (2026A for D, 2026B for C). The desired elevation range is >30 degrees for Q, Ka, and K observations, while >20 degrees is acceptable for Ku and X bands. There are no coordinated or fixed-date observations or other constraints in that sense. We estimate 45 total passes (including all bands) in the LST ~ 0-9h range to complete the program (~6 in Q, ~7 in Ka, ~11 in K, ~9 in Ku, and ~12 in X).

LST Range Justification:

N/A

Receivers requested:

To cover the full broadband spectra of the targets from ~10-45 GHz we are proposing to observe each target in the Q, Ka, K, Ku, and X bands with coarse (continuum) spectral resolution, averaging spectral windows as needed to achieve the desired signal-to-noise ratio (SNR).

Samplers and correlator setup:

We will use the 3-bit samplers to maximize simultaneous continuum bandwidth. The standard continuum setup is sufficient for our purposes.

Mosaic requirements:

These are single-pointing observations: no mosaicking or OTF mapping are needed.

Sensitivity:

We targeted noise levels in each band based on the expected flux densities of the targets extrapolated from higher frequencies, roughly targeting fixed SNRs in each band (SNR = 8 in Q and Ka, SNR = 5 in K, Ku, and X) that were optimized through injection/recovery tests for modeling spectra (described in detail in the Scientific Justification). Each source has its own target sensitivity (RMS) in each band, based on these extrapolations and target SNRs (appropriately adjusted to match minimum target-calibrator cycle times). In assessing these target noise levels, we considered the effectively diminished bandwidths (10-15%) in Ku and X bands from RFI and the variations in sensitivity expected across each band. The data are designed to be sensitivity-limited.

Integration time:

The required on-source time is different for each target, depending on the expected flux and desired SNR based on the calculations and modeling described in the Scientific Justification. The times are adjusted as appropriate so the observations of each target fit in an integer number of the minimum target-calibrator cycles times for each band. The Ku and X-band estimates are increased to improve the RMS by 10% to compensate for potential RFI losses. The program is designed to take advantage of the proximity of large groups of targets on the sky. We will observe many targets together in each (~2 hour) SB that will share a calibrator. There is not an appropriate "representative" target for an ECT example in each band. However, the on-source times scale as expected with the desired RMS. And the appropriate overhead estimates correspond to the total on-source time in a typical SB. So we provide here appropriate examples based on that principle, using an on-source time of 1 hour to guide the reviewers. In some cases, that 1 hour will be for a single source; but usually it will be shared for many sources. We note that the added slew times are considered in how we discretize the on-source time into target-calibrator cycles (though they are quite small for this program). The corresponding on-source time for a given desired RMS will scale with 1 / RMS**2, but the effective overhead rate (t_total / t_source) shown there can be used to scale the total time requests (as used in the sessions).

For the group 3 sessions, we account for the inefficiency of shorter observations as appropriate (using the overheads required for the shorter on-source times for those few targets).

Dump time:

The default dump time of 3 s is appropriate for this program. The default data rates for this setup are 15.8 MB/s (Q, Ka, K), 11.8 MB/s (Ku), and 7.9 MB/s (X). We estimate the raw data volume (accounting for all observing, aside from slew times estimated in overheads) will be ~14 TB in total.

Imaging considerations:

The only real issue for this program is associated with the wide fractional bandwidth. We will explore splitting the data into 2-4 GHz sub-bands and imaging each with standard CASA routines and compare the returns on spectral fitting against flux estimates from the Taylor expansion imaging capabilities inside CASA (over the full bandwidths).

Polarimetric considerations:

N/A

RFI considerations:

RFI in the X, and Ku bands may affect ~10-15% of the bandpass, but standard flagging can excise the problematic data. This has been considered in estimates of the desired sensitivities (as noted in the RMS comments).

Joint considerations:

Mapping area (Single Pointing/ Multiple pointings/Rectangular Mosaic of given area):
Multiple Pointings.

Required 12 m Array configuration(s):
The purpose is unresolved photometry, with target emission sizes expected to be <~1.5" in diameter at 100 GHz. Configurations C-1 to C-4 are suitable.

Requested angular resolution and largest angular scale (in arcseconds):
Angular resolution <= 1.5". The targets will be unresolved, so the largest angular scale is similar.

Time request considering overheads (Times calculated with Observing Tool already include overheads)

12 m Array: 7 hours.
7 m Array: N/A
TP: N/A

Requested Band(s):
Band 3

Representative sensitivity for reference array (i.e. 12m, or 7m for ACA stand-alone projects) and aggregated bandwidth used for sensitivity calculation:
We split the sample targets (calibrators can be shared, since all targets are at similar sky locations) into 3 Science Goals to provide roughly constant signal-to-noise ratios, with RMS sensitivity requests of 30, 45, and 85 microJy. In all cases we assume the total dual-polarization TDM continuum bandwidth (7.5 GHz).

Is the time request resulting from OT:
Yes.

Report here the highest spectral and imaging signal-to-noise ratios expected in your sample:
This is a continuum only program, so spectral signal-to-noise is not relevant. The highest imaging signal-to-noise expected is ~300 (though the typical value will be ~25).

Is full-polarization required?
No.

The coordinates of any source with a declination northern than +30deg:
04:55:45.85, +30:33:04.29
04:55:59.39, +30:34:01.50

The expected source linear/circular polarization fraction:
0

Other:
N/A

Purpose	25A (typical SB)
Array Configuration	C
Number of Antennas	25
Polarization Setup	Dual
Number of Sources	1
Type of Image Weighting	Natural
Representative Frequency	15.0000 GHz
Receiver Band	Ku
Approximate Beam Size	2.092"
Digital Samplers	3 bit
Elevation	High (50°-90°)
Average Weather	Summer
Calculation Type	Noise/Tb
Time on Source	1h 0m 0s
Total Time	1h 42m 53s
Frequency Bandwidth	6.0000 GHz
Line Velocity Width	119,916.9832 km/s
RMS Noise (units/beam)	2.4536 µJy
RMS Brightness (temp)	0.0030 K
Confusion Level	0.0070 µJy

Overhead. Short high-frequency observations: overhead calculated as T_oh = 0h 42m 52.8s = 0.348 * 1h 0m 0s + 0h 22m 0s, with the fixed overhead consisting of an initial slew of 0h 11m 0s and a fixed calibration and pointing overhead of 0h 11m 0s.

Severe RFI effects. At this frequency band, part of the selected bandwidth may be severely affected by RFI. Visit the following web page for the RFI information at the VLA: https://science.nrao.edu/facilities/vla/docs/manuals/obsguide/modes/rfi Of the 12-18 GHz frequency span of the Ku-band, up to 12% could be affected by RFI. This should be properly accounted for while estimating the rms noise.

Produced by the NRAO EVLA Exposure Calculator (2023 December).

Purpose	25A (typical SB)
Array Configuration	D
Number of Antennas	25
Polarization Setup	Dual
Number of Sources	1
Type of Image Weighting	Natural
Representative Frequency	44.0000 GHz
Receiver Band	Q
Approximate Beam Size	2.354"
Digital Samplers	3 bit
Elevation	High (50°-90°)
Average Weather	Winter
Calculation Type	Noise/Tb
Time on Source	1h 0m 0s
Total Time	1h 51m 46s
Frequency Bandwidth	8.0000 GHz
Line Velocity Width	54,507.7196 km/s
RMS Noise (units/beam)	8.6730 μJy
RMS Brightness (temp)	0.0010 K
Confusion Level	0.0042 μJy

Overhead. Short high-frequency observations: overhead calculated as T_oh = 0h 51m 45.6s = 0.496 * 1h 0m 0s + 0h 22m 0s, with the fixed overhead consisting of an initial slew of 0h 11m 0s and a fixed calibration and pointing overhead of 0h 11m 0s.

Samplers have been switched to 3-bit. The calculations now reflect the use of the 3-bit digital samplers. Compared to the 8-bit samplers there is about a 15% sensitivity penalty when using the 3-bit samplers.

Produced by the NRAO EVLA Exposure Calculator (2023 December).

Purpose	25A (typical SB)
Array Configuration	D
Number of Antennas	25
Polarization Setup	Dual
Number of Sources	1
Type of Image Weighting	Natural
Representative Frequency	33.0000 GHz
Receiver Band	Ka
Approximate Beam Size	3.138"
Digital Samplers	3 bit
Elevation	High (50°-90°)
Average Weather	Winter
Calculation Type	Noise/Tb
Time on Source	1h 0m 0s
Total Time	1h 47m 16s
Frequency Bandwidth	8.0000 GHz
Line Velocity Width	72,676.9595 km/s
RMS Noise (units/beam)	4.2616 µJy
RMS Brightness (temp)	0.0005 K
Confusion Level	0.0167 µJy

Overhead. Short high-frequency observations: overhead calculated as T_oh = 0h 47m 15.6s = 0.421 * 1h 0m 0s + 0h 22m 0s, with the fixed overhead consisting of an initial slew of 0h 11m 0s and a fixed calibration and pointing overhead of 0h 11m 0s.

Samplers have been switched to 3-bit. The calculations now reflect the use of the 3-bit digital samplers. Compared to the 8-bit samplers there is about a 15% sensitivity penalty when using the 3-bit samplers.

Produced by the NRAO EVLA Exposure Calculator (2023 December).

Purpose	25A (typical SB)
Array Configuration	D
Number of Antennas	25
Polarization Setup	Dual
Number of Sources	1
Type of Image Weighting	Natural
Representative Frequency	22.0000 GHz
Receiver Band	K
Approximate Beam Size	4.707"
Digital Samplers	3 bit
Elevation	High (50°-90°)
Average Weather	Winter
Calculation Type	Noise/Tb
Time on Source	1h 0m 0s
Total Time	1h 47m 16s
Frequency Bandwidth	8.0000 GHz
Line Velocity Width	109,015.4393 km/s
RMS Noise (units/beam)	3.8860 μJy
RMS Brightness (temp)	0.0004 K
Confusion Level	0.0717 μJy

Overhead. Short high-frequency observations: overhead calculated as T_oh = 0h 47m 15.6s = 0.421 * 1h 0m 0s + 0h 22m 0s, with the fixed overhead consisting of an initial slew of 0h 11m 0s and a fixed calibration and pointing overhead of 0h 11m 0s.

Samplers have been switched to 3-bit. The calculations now reflect the use of the 3-bit digital samplers. Compared to the 8-bit samplers there is about a 15% sensitivity penalty when using the 3-bit samplers.

Produced by the NRAO EVLA Exposure Calculator (2023 December).

Purpose	25A (typical SB)
Array Configuration	C
Number of Antennas	25
Polarization Setup	Dual
Number of Sources	1
Type of Image Weighting	Natural
Representative Frequency	10.0000 GHz
Receiver Band	X
Approximate Beam Size	3.137"
Digital Samplers	3 bit
Elevation	High (50°-90°)
Average Weather	Summer
Calculation Type	Noise/Tb
Time on Source	1h 0m 0s
Total Time	1h 27m 38s
Frequency Bandwidth	4.0000 GHz
Line Velocity Width	119,916.9832 km/s
RMS Noise (units/beam)	2.6768 µJy
RMS Brightness (temp)	0.0033 K
Confusion Level	0.0394 µJy

Overhead. Short low-frequency observations: overhead calculated as T_oh = 0h 27m 38.4s = 0.244 * 1h 0m 0s + 0h 13m 0s, with the fixed overhead consisting of an initial slew of 0h 11m 0s and a fixed calibration overhead of 0h 2m 0s.

Severe RFI effects. At this frequency band, part of the selected bandwidth may be severely affected by RFI. Visit the following web page for the RFI information at the VLA: https://science.nrao.edu/facilities/vla/docs/manuals/obsguide/modes/rfi Of the 8-12 GHz frequency span of the X-band, up to 15% could be affected by RFI. This should be properly accounted for while estimating the rms noise.

Produced by the NRAO EVLA Exposure Calculator (2023 December).

1. Motivation and Background

The formation of planets in the canonical core accretion model depends critically on the reservoir of solid mass in the progenitor circumstellar disk and the growth of those solids from μm-sized dust grains to km-scale planetesimals [1,2,3]. Information about disk solids is accessed through the $\sim$20–500 GHz thermal continuum spectrum emitted by dust [4]. If the optical depths are low, the continuum flux S_ν scales with mass [5], and the spectral index (α, where $S_\nu \propto \nu^\alpha$) traces the shape of the opacity spectrum κ_ν ($\alpha \approx 2+\beta$ in the Rayleigh-Jeans limit, where $\kappa_\nu \propto \nu^\beta$; [6]), and thereby the grain size distribution [7]. Constraints on these fundamental metrics for planet formation have come from ALMA surveys that track how S_ν and α evolve and depend on other properties [8].

For standard assumptions, the observed S_ν distribution for $\sim$1–3 Myr-old disks implies there is not enough progenitor mass available (by a factor of $\sim$3) to explain the exoplanet population [9], driving speculation that planet formation finished early [10,11] or that mass is replenished from the environment [12]. A more mundane possibility is that a significant fraction of S_ν – usually measured at 230 or 340 GHz – is optically thick. In optically thick regions, brightness temperatures saturate at the local dust temperatures, or lower if the albedos are high [13]. In this case, S_ν is insensitive to mass (it sets only a lower limit) and α is insensitive to the particle sizes ($\alpha \approx 2$; see [14]).

There is compelling evidence that high optical depths (at $\nu \gtrsim 100$ GHz) bias disk mass estimates [e.g., 15]. At high resolution, the continuum often exhibits high brightness temperatures [16] but shallow spectra ($\alpha \approx 2$; [17,18]), particularly within a few tens of au of the host stars and/or in small-scale "substructures". At coarser resolution, larger samples show S_ν is correlated with the square of the emission size (i.e., the disk surface area; [19]), as expected if optical depths are high. While dust evolution population synthesis models can explain this scaling with optically thin emission [20,21], they predict much steeper spectra ($\alpha > 3$) than are observed ($\alpha \approx 2.2$; [22]). A modified set of these models reproduces the S_ν–size scaling and the low α values by concentrating dust into localized substructures with high optical depths [23].

Vetting these predictions is now essential, since such models offer a physical framework that may substantially shift how we interpret continuum emission. More generally, **an accurate assessment of disk masses, and thereby planet formation potential, requires access to optically thin emission**. Given the potentially high optical depths at $\nu \gtrsim 100$ GHz, **the only viable approach is to extend our continuum measurements to lower frequencies**, where the optical depths are diminished.

2. Goals and Request

We propose a VLA Large Program to measure 10–45 GHz continuum spectra for a large sample of protoplanetary disks in the $\sim$1–3 Myr-old Taurus region. Specifically, we request 385 hours in the Q/Ka/K/Ku/X bands, split in the C and D configurations, for deep photometry of 78 targets. We also request a 7 hour complementary census of the same targets in ALMA Band 3 (100 GHz), to ensure data of uniform quality are available to probe if the spectral shape changes as the optical depths decrease. This survey will provide a pathfinder catalog for nearby, northern-sky disks to guide plans for future imaging surveys with the ngVLA. Significantly, it will be the largest sample of cm-band disk spectra to cover the full range of some key parameters in planet formation models.

3. Why a Large Sample?

Demographic trends associated with the mm (230–340 GHz) continuum fluxes ($S_{\rm mm}$) are guiding the theoretical development of planet formation models (see [8]). An overlapping sample at lower

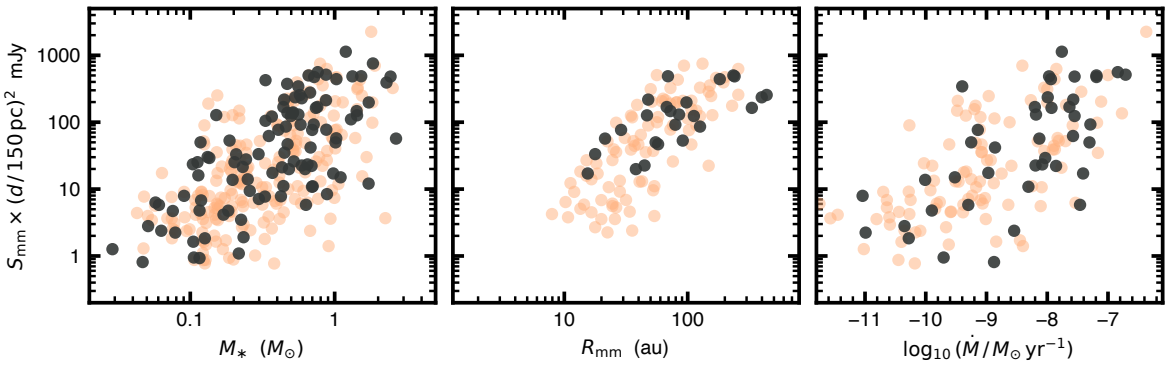

Figure 1: The key demographic trends associated with mm emission in nearby ∼1–3 Myr-old disk populations, including scalings between S_{mm} (corrected for distance d) and M_* (left), R_{mm} (middle), and $\dot{M}$ (right). Black points are Taurus disks, the focus of this program; orange points include disks from other similar regions in the southern sky (Lup, Oph, and Cha). Two conflicting interpretations can explain these demographic trends equally well. [*Data collated from [4,8].*]

frequencies that spans the same ranges of fundamental parameters is imperative to assess how optical depth affects these trends. More practically, we need to understand the behavior of disks in the cm bands for a less biased sample to effectively plan for the ngVLA.

Figure 1 shows that S_{mm} scales with stellar host mass M_* [24], mm continuum size R_{mm} [19,25], and accretion rate $\dot{M}$ [26] for nearby disk populations. Two competing interpretations of these trends have emerged from disk population synthesis models. The 'evolution' option predicts the mm continuum is mostly optically thin, so S_{mm} is a proxy for mass. Then, the $S_{mm}-M_*$ scaling traces an intrinsic disk–star mass relation, accounting for the $S_{mm}-\dot{M}$ scaling through classical viscous theory and the $S_{mm}-R_{mm}$ scaling from the inward migration of dust [20,21]. In this case, planet formation is slower, and occurs preferentially in the inner disk ($\lesssim$ 10 au). The 'substructures' option instead predicts the mm continuum is optically thick because migrating dust becomes trapped in local pressure maxima [23]. This alternative assumes that disks around more massive stars make those substructures at larger radii, creating the $S_{mm}-R_{mm}$ scaling. The $S_{mm}-M_*$ trend arises from that scaling and the connection between stellar luminosities (which scale like $M_*^{1.5}$) and disk heating, and the $S_{mm}-\dot{M}$ trend is tied to an intrinsic $M_*-\dot{M}$ relation (see [27]). In this case, planet formation happens quickly, and perhaps even at large radii (to ∼100 au).

4. Expectations and Analysis Plans

These options for explaining the demographic trends represent two fundamentally different ideas about what the mm continuum *means* – is it a mass tracer or not? Considering how closely we tie such measurements of disks to technical optimizations and justifications for our current (ALMA) and future (ngVLA) facilities, it seems important to figure this out. To do that, we have a baseline analysis plan with straightforward goals. We will measure the dust contributions (see Sect. 5) to the ∼30 GHz (1 cm) continuum fluxes (S_{cm}^d) and the 30–100 GHz spectral indices (α_{cm}^d) for a large and diverse sample, compare to their mm-band counterparts (S_{mm} and α_{mm}), and assess their behavior as a function of M_* or $\dot{M}$,[1] in the context of the population synthesis models.

[1]While R_{cm} would also be valuable, the few targets observed so far show $R_{cm} \ll R_{mm}$ [28,29,30], presumably due to very low surface brightnesses. A diverse sample of R_{cm} requires the ngVLA.

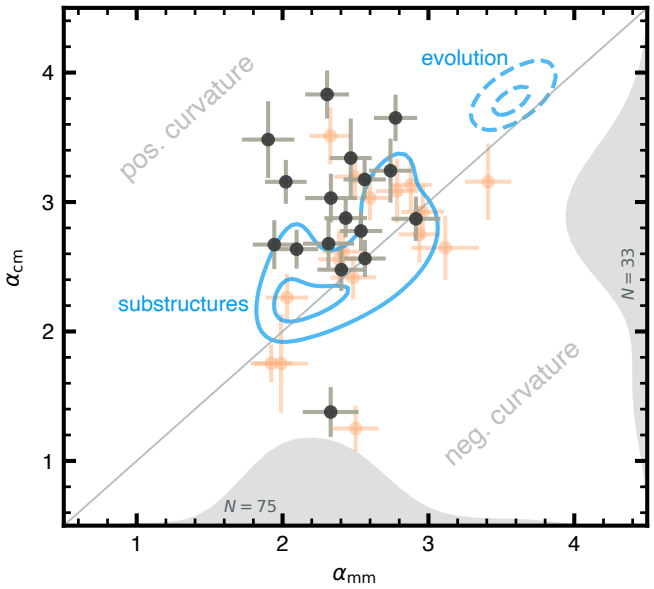

Figure 2: A representation of the spectrum *curvature* on either side of 100 GHz (including any contamination; see Sect. 5), for literature data of disks in Taurus (black) and similar regions (orange). Note that $\alpha_{\rm cm}$ measurements are still rare, and limited to very bright disks. The distributions (using kernel density estimators) of all available measured indices (including targets in Tau, Lup, Cha, Oph) are shown along the axes (the numbers of included disks are marked). Contours enclosing 25 and 75% for two sets of population synthesis models are marked for reference [21,23]. [*Data from [4,22,31,32,33,34].*

Figure 2 focuses on the spectrum *curvature*: the variation of the spectral index with frequency is the key controlling factor and clue to the behavior of demographic trends in $S^d_{\rm cm}$. If all disks had the same curvature, the cm trends would be scaled versions of the mm ones. But if, for example, $\alpha^d_{\rm cm}$ increases with M_*, we would see a flatter $S^d_{\rm cm} - M_*$ relation than in the mm.

The default population synthesis models predict little curvature ($\alpha_{\rm cm} \approx \alpha_{\rm mm}$), although they are centered around very different indices ($\sim$3.5 vs. 2.2). Indeed, the 'evolution' models are in conflict with the observed $\alpha_{\rm mm}$ distribution. While shifting those predictions by changing the typical dust porosity or composition is possible, it is unclear if such modifications could still successfully account for the mm demographic trends. The 'substructure' models remain mostly optically thick at 33 GHz. If that is the general case, it would imply that disk mass estimates are $\gtrsim 3\times$ too low (for the standard κ_ν ratio between 33 and 340 GHz) and the 'missing mass' problem (Sect. 1) is solved.

Positive curvature ($\alpha_{\rm cm} > \alpha_{\rm mm}$) would imply the spectrum transitions from *marginally* optically thick to thin around 100 GHz. Then, measurements of $S^d_{\rm cm}$ and $\alpha^d_{\rm cm}$ would be much less biased tracers of the dust masses and opacity spectra (β), and we can place the demographic relationships on a more robust physical footing. Interestingly, the 'substructure' models can naturally accommodate this scenario. The dust concentrations in these models are high enough to trigger the streaming instability [35], rapidly converting small particles into large planetesimals. This planetesimal formation threshold self-regulates to maintain optical depths of $\sim$1–10 at $\nu \gtrsim 100$ GHz [36]. In that case, the cm-band measurements would reveal the remnant mass of the planetesimal 'feedstock', and a revised population synthesis model with a planetesimal formation algorithm and tuned to reproduce the VLA data would constrain the "missing" mass hidden in planetesimals.

Spectra with negative curvature ($\alpha_{\rm cm} < \alpha_{\rm mm}$) are contaminated *by a different emission mechanism*. Mitigating such contamination is our fundamental technical challenge, as explained below.

5. Spectrum Measurements

Potential contamination sources include bremsstrahlung from winds or outflows [37,38], gyrosynchrotron radiation from active stellar coronae [39], or electric dipole emission from spinning dust [40,41]. Each of these has a different spectral shape from the dust disk: bremsstrahlung is flat to

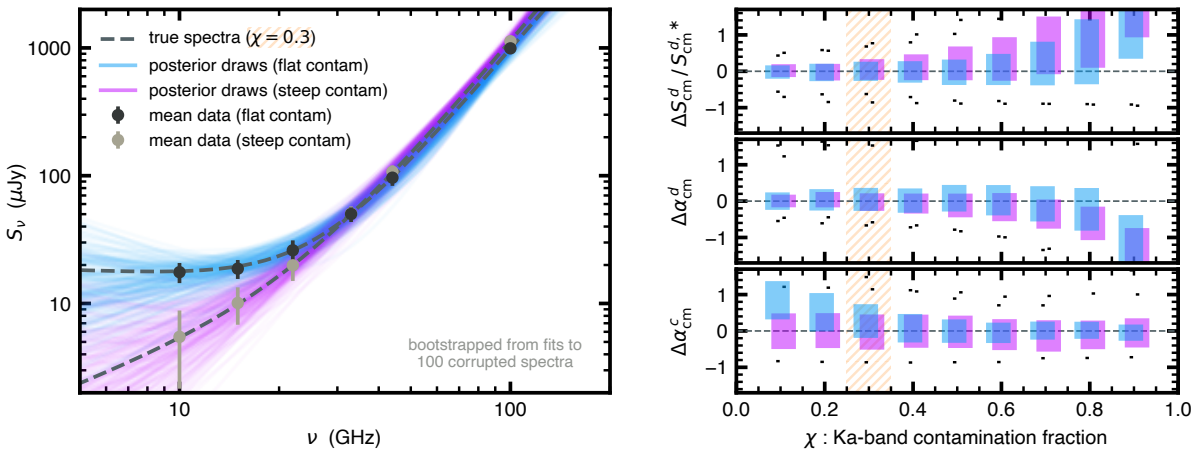

Figure 3: The left panel shows fits to two illustrative types of synthetic spectra (a composite of 100 realizations for spectra corrupted by appropriate noise and calibration uncertainties). In blue (data as black points), we show posterior draws from fits to a model with $\alpha^d_{\rm cm} = 3.0$, $\alpha^c_{\rm cm} = 0$, and in purple (data as gray points) a model with $\alpha^d_{\rm cm} = 3.2$, $\alpha^c_{\rm cm} = 1$. Both cases have $\chi = 0.3$ (30% contamination in Ka) and $S_{\rm cm} = 50$ μJy. Note that these results are scalable with $S_{\rm cm}$, since the survey is designed with ∼uniform SNR. The right panels show the quality of the retrievals for similar models with different χ. The top row shows the fractional deviations with respect to the true (injected) *dust* contributions to $S_{\rm cm}$, the middle and bottom rows the differences between the inferred and injected $\alpha^d_{\rm cm}$ and $\alpha^c_{\rm cm}$, respectively. Each box represents the 68% uncertainties.

rising ($\alpha^c_{\rm cm} \approx 0$ to 1); gyrosynchrotron is falling ($\alpha^c_{\rm cm} \approx -1$ to 0); and spinning dust produces a "bump" at ∼20–40 GHz. Consensus in the field is that bremsstrahlung is most common, but this is based on sparsely-sampled spectra in a biased sample (bright disks with high M_*, $R_{\rm mm}$, and $\dot{M}$). An honest assessment is that we do not know what to expect in the broader population.

In any case, we need to disentangle the dust contribution (at Ka and Q) from any contamination. Assuming both contributors have power-law spectra, we can define a simple model

$$S_\nu = (1-\chi)S_{\rm cm}\left(\frac{\nu}{33\,{\rm GHz}}\right)^{\alpha^d_{\rm cm}} + \chi S_{\rm cm}\left(\frac{\nu}{33\,{\rm GHz}}\right)^{\alpha^c_{\rm cm}}, \quad (1)$$

where $S_{\rm cm}$ is the total Ka flux, $\alpha^d_{\rm cm}$ and $\alpha^c_{\rm cm}$ are the indices for the dust and contamination, and χ is the contaminated fraction at Ka, so $S^d_{\rm cm} = (1-\chi)S_{\rm cm}$ and $S^c_{\rm cm} = \chi S_{\rm cm}$ (the contamination term could be adjusted in the case of spinning dust, swapping the index out for a "bump" center and width). We designed a large suite of injection/recovery tests to quantify our ability to disentangle the two contributions for various parameters, types and levels of contamination, observing bands, and signal-to-noise ratios (SNRs; with some feedback from the strategy and selection exercise in Sect. 6). For each set of options, we generated 100 synthetic spectra corrupted by the expected noise (including flux calibration ambiguities), modeled each of those to sample posteriors on {$S_{\rm cm}$, χ, $\alpha^d_{\rm cm}$, $\alpha^c_{\rm cm}$}, and then combined the results to estimate the expected quality of the retrievals.

Figure 3 offers a representative illustration of our conclusions from these injection/recovery tests. For the conservative assumption of bremsstrahlung contamination (i.e., the faintest option at low frequencies), the proposed survey can faithfully recover the correct $S^d_{\rm cm}$ and $\alpha^d_{\rm cm}$ with good precision when the majority of the Ka-band emission is from dust ($\chi \lesssim 0.5$). For the data in the literature so far, this is >90% of the cases (though we do note again the sample bias). The key is to have robust

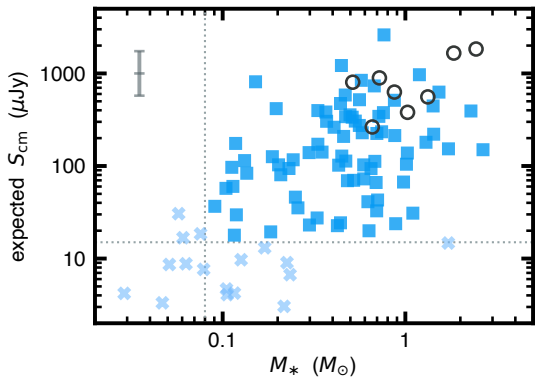

Figure 4: The expected Ka fluxes for Taurus disks as a function of M_*. The sample targets are shown as blue squares, existing data with black circles, and excluded targets with light blue '×' symbols. The selection criteria (marked with dotted lines) do not significantly diminish the M_* (or $\dot{M}$) diversity in the sample. The error bar in the upper left denotes varying the adopted α_{cm} by ±0.5.

measurements (or strong upper limits) of the complete spectrum from ∼10–100 GHz. The 100 GHz data are especially important if $\chi \gtrsim 0.2$: without that access to a less-contaminated frequency, the precision and accuracy for a constraint on α^d_{cm} (and thus S^d_{cm}) are substantially diminished. **A common approach has been to cut corners on the K, Ku, X bands that probe the contamination to reduce observing costs, but we find that this compromises the constraints on $\{\chi, \alpha^c_{cm}\}$ such that inferences of the dust spectrum appear precise, but are inaccurate.** For example, removing any one of those bands from the experiments in Figure 3 ($\chi = 0.3$) expands the parameter degeneracies and biases the retievals of α^d_{cm} down by ∼0.2–0.4 and S^d_{cm} up by ∼30–50%.

While that illustrates how the K, Ku, and X-band data are essential for marginalizing out the contamination, they will also let us precisely characterize that radio emission for a larger sample of young stars in cases with $\chi \gtrsim 0.3$. This can be a key resource for ngVLA planning, and will help us better link accretion, outflows, and stellar activity in such systems [e.g., 42,43].

6. Observing Strategy and Sample Selection

The goal in sample selection was to span the full ranges of the mm demographic trends (primarily in M_*), to re-assess them in the cm emission. This requires a large sample size, to ensure we can quantify those trends even with the significant scatter seen in the mm relations (and measure that scatter). We started with the 147 Class II disks in Taurus. We removed close binaries, targets with no previous mm data, and brown dwarfs (a cut at $M_* > 0.08 M_\odot$). This leaves 95 potential targets. We recently made similar observations (22A-179) for 8 of these that do not need to be repeated.

We next estimated *expected* fluxes using extrapolations from 100 GHz. Class II disks with existing 100 GHz data have $\alpha_{mm} \approx 2.2$ ([22]; see Fig. 2). There is a slight preference for higher α_{mm} at larger M_*, due to a prevalence of transition disks (with depleted central regions, and thus lower optical depths). For Taurus targets without such data, we estimated 100 GHz fluxes by extrapolating from 230/340 GHz, adopting $\alpha_{mm} = 2$ when $M_* \leq 0.35 M_\odot$ and increasing as $M_*^{0.2}$ at higher M_*. Then, we assumed $\alpha_{cm} = 3$ to estimate Q and Ka fluxes, the mean behavior in Figure 2. The expected fluxes in K, Ku, and X assumed $\alpha^c_{cm} = 0$ and $\chi = 0.2$. Using the injection/recovery tests described above, we set minimum SNR requirements of 25 at 100 GHz, 8 at Q and Ka, and 5 in K, Ku, and X. We then calculated on-source times, adjusting as appropriate so each target is observed for an integer number of target-calibrator cycles. Figure 4 shows the expected Ka fluxes.

To balance costs against the returns of adding fainter targets, we opted to exclude targets with predicted Ka-band fluxes <15 μJy, removing an additional 9 targets to leave a full sample of 78 (plus the 8 already in-hand from 22A-179). To give some context for this final cut: shifting the boundary to 10 μJy would add 2 more targets, but cost 110 hours. Since excluding these targets

does not change the sampled range of M_* (or $\dot{M}$), this is a natural breakpoint. Archival VLA data exist for 23 of these targets, although not with the depth or frequency coverage needed for our purposes and preferentially for bright, "low-cost" targets. Those data can be useful for quantifying any variability in the contamination spectra (typically found to be small, e.g., by comparing [31] to our 22A-179 data). Applying the standard overhead rates in the ECT, the total VLA time request is ∼385 hours: 47 in Q, 63 in Ka, 95 in K, 76 in Ku, and 104 in X. The total time request for the complementary joint observations with ALMA in Band 3 is 7 hours.

7. Plan for Data Reduction and Release

Our team includes experienced VLA and ALMA users (Andrews, Chandler, Wilner, Macias, Carrasco-Gonzalez, Long, Liu). We expect all the data will be calibrated in the standard pipelines. We will split up the tasks of self-calibration (when possible) and standard imaging among the team. The goal is to train a CfA graduate student in VLA calibration and analysis with this program. After calibration, flux measurements in each band are straightforward (simple point-like models in the image and/or visibility domains). The goal will be to have flux measurements determined within a month or two of the observations being pipeline-processed (depending on the delivery rate).

Given the configuration schedule, we understand that we may have to wait some time for measurements of all targets/bands to be complete; there is no requirement that the data are obtained within a single configuration cycle, if that eases scheduling constraints. The analysis procedure is already worked out (cf., Fig. 3), so the aim is to disentangle the spectra and infer the parameters of interest shortly after the data are calibrated. We will aim for an initial publication within the proprietary period that provides the key measurements and releases the images, fluxes, spectral indices, and associated posterior samples in digital form (on Zenodo). Meanwhile, we will complete publications about the demographics (student/all), physical constraints from opacity modeling (Ueda), and broader implications in the context of new population synthesis models (Birnstiel).

References

[1] - Pollack et al. 1996, *Icarus*, 124, 62 • [2] - Birnstiel et al. 2016, *SSRev*, 205, 41 • [3] - Drążkowska et al. 2023, *PPVII*, 2203.09759 • [4] - Andrews 2020, *ARA&A*, 58, 483 • [5] - Beckwith et al. 1990, *AJ*, 99, 924 • [6] - Beckwith & Sargent 1991, *ApJ*, 381, 250 • [7] - Draine 2006, *ApJ*, 636, 1114 • [8] - Manara et al. 2023, *PPVII*, 2203.03930 • [9] - Manara et al. 2018, *A&A*, 618, L3 • [10] - Greaves & Rice 2011, *MNRAS*, 412, L88 • [11] - Najita & Kenyon 2014, *MNRAS*, 445, 4315 • [12] - Throop & Bally 2008, *AJ*, 135, 2380 • [13] - Zhu et al. 2019, *ApJ*, 877, L18 • [14] - Liu 2019, *ApJL*, 877, 22 • [15] - Xin et al. 2023, *ApJ*, 942, 4 • [16] - Huang et al. 2018, *ApJ*, 852, 122 • [17] - Tsukagoshi et al. 2016, *ApJL*, 829, 35 • [18] - Long et al. 2020, *ApJ*, 898, 36 • [19] - Tripathi et al. 2017, *ApJ*, 845, 44 • [20] - Rosotti et al. 2019, *MNRAS*, 486, L63 • [21] - Zormpas et al. 2022, *A&A*, 661, 66 • [22] - Tazzari et al. 2021, *MNRAS*, 506, 5117 • [23] - Delussu et al. 2024, *A&A*, 2405.14501 • [24] - Andrews et al. 2013, *ApJ*, 771, 129 • [25] - Andrews et al. 2018, *ApJ*, 865, 157 • [26] - Manara et al. 2016, *A&A*, 591, L3 • [27] - Hartmann et al. 2016, *ARA&A*, 54, 135 • [28] - Pérez et al. 2012, *ApJL*, 760, L17 • [29] - Tazzari et al. 2016, *A&A*, 588, 53 • [30] - Tripathi et al. 2018, *ApJ*, 861, 64 • [31] - Rodmann et al. 2006, *A&A*, 446, 211 • [32] - Ubach et al. 2012, *MNRAS*, 425, 3137 • [33] - Ubach et al. 2017, *MNRAS*, 466, 4083 • [34] - Curone et al. 2023, *A&A*, 677, 118 • [35] - Youdin & Goodman 2005, *ApJ*, 620, 459 • [36] - Stammler et al. 2019, *ApJ*, 884, L5 • [37] - Reynolds 1986, *ApJ*, 304, 713 • [38] - Pascucci et al. 2012, *ApJL*, 751, 42 • [39] - Chiang et al. 1996, *AJ*, 111, 355 • [40] - Rafikov 2006, *ApJ*, 646, 288 • [41] - Hoang et al. 2018, *ApJ*, 862, 116 • [42] - Purser et al. 2018, *MNRAS*, 481, 5532 • [43] - Pascucci et al. 2018, *ASPC: Science with the ngVLA*, 517, 155